



Influence of temperature on hydration and microstructure properties of limestone-calcined clay blended cement

Geetika Mishra · Arun C. Emmanuel · Shashank Bishnoi

Received: 6 January 2019 / Accepted: 20 August 2019
© RILEM 2019

Abstract In this article, the strength and microstructure development of two low clinker blended cements; limestone calcined clay cement (LC^3) and slag-fly ash composite cement (CC) cured at 27 °C and 50 °C are analysed and compared to those of ordinary Portland cement (OPC). A significant difference in the 28 days strength was observed between 27 and 50 °C cured specimens in low clinker blends. The results show that the quantities of ettringite and carbo-aluminate phases significantly reduce when LC^3 is cured at 50 °C. EDX analysis shows that significant quantities of aluminate are taken up in C–A–S–H, when curing is done at a higher temperature. It was seen from BSE image analysis that the C–A–S–H formed from the hydration of LC^3 is much more heterogenous than the other cements due to non-uniformity in C–A–S–H density as well as intermixing of hydration products. It was also seen that although an increase in the temperature leads to a measurable increase in the density of C–S–H in

OPC and CC, the influence on LC^3 is not clear, the heterogeneity of the product appears to reduce. In the case of both LC^3 and CC, the hydration of clinker is slowed down, especially after the first day, when cured at 50 °C. All these factors lead to a coarsening of the pore-structure and a reduction in the compressive strength of both low clinker cements, when cured at the higher temperature.

Keywords Low clinker cements · Curing temperature · Calcined clay · C–A–S–H

1 Introduction

Concretes containing supplementary cementitious materials (SCMs) are used extensively throughout the world for their good performance, economic and environmental benefits. The most common SCMs are fly ash, ground granulated blast furnace slag, limestone, silica fume and calcined clay. Several performance benefits, such as energy, and resource conservation, lower CO₂ emissions, etc., have been reported from the use of these SCMs [1]. Temperature plays an important role on the hydration characteristics of SCMs blended cements. Although the sensitivity of hydration of ordinary Portland cement (OPC) and blended cements is well documented in the literature [2, 3], such studies on low clinker cements (containing 50% or less of clinker) such as limestone

Electronic supplementary material The online version of this article (<https://doi.org/10.1617/s11527-019-1390-5>) contains supplementary material, which is available to authorized users.

G. Mishra · A. C. Emmanuel (✉) · S. Bishnoi
Indian Institute of Technology Delhi, New Delhi, India
e-mail: aruncemmanuel@gmail.com

G. Mishra
e-mail: geetika.mishra30@gmail.com

S. Bishnoi
e-mail: bishnoi@iitd.ac.in



calcined clay cement (LC^3) and fly ash-slag composite cements were not found. Change in temperature affects the mechanical properties of hydrated cementitious systems. It is well reported that when OPC is cured at a higher temperature, the rate of strength development is reduced at later ages. This effect is directly related to the change in the properties of the hydration products and the process of microstructural development at higher temperatures [4–7]. It has been reported that the microstructure is more heterogeneous and that the density of calcium silicate hydrate (C–S–H) is higher due to the faster hydration at higher temperatures [8]. A destabilization of ettringite and monocarbonate to monosulphoaluminate and calcite also takes place [2]. This change leads to a coarsening of the pores and can potentially reduce the strength performance of the mix [8–10]. At lower temperatures, the rate of hydration is reduced, providing more time for ions to diffuse before the precipitation of the hydration products. This leads to the development of C–S–H gel with a lower polymerisation and a higher gel-porosity [11–14]. This change in C–S–H structure contributes to the formation of a microstructure with more uniform distribution of hydration products, which reduces the coarser pores and increases the compressive strength [15, 16].

Several authors have reported a change in the grey level of C–S–H at different temperatures using backscattered electron imaging (BSE images) [17–20]. This change in grey level could be due to the change in density of C–S–H caused by change in its composition [21, 22]. However, conflicting results have been reported on change in elemental composition due to temperature. Some studies indicated that the Ca/Si ratio is not affected up to 75 °C [11, 23] while others reported a change in Ca/Si ratio against curing temperature, which could be due to multiple reasons such as intermixing of CH or higher sulphate adsorption with elevated temperature [22, 24–26]. The increase in sulphate adsorption in C–S–H at higher temperature could be due to the dissolution of ettringite at elevated temperature leading to increase in sulphate concentration in pore solution [10, 17, 27]. An increase in degree of polymerisation of silicate chains with temperature has been observed [28]. Apart from silicate polymerization, a reduction of interlayer water and subsequent reduction of spacing between interlayers of C–S–H was also observed [29]. This leads to formation of a denser C–S–H, leading to

increase in capillary porosity and decrease in gel porosity in cement matrix [30].

Generally, the addition of SCMs accelerates the early age hydration of clinker phases due to filler and dilution effects. The surface of SCMs provide additional nucleation sites for the precipitation of C–S–H, leads to a faster hydration of the clinker phases. This is known as the filler effect. Also, the partial replacement of clinker by an SCM increases the water available for the clinker phases, increasing their dissolution and the space available for the growth of the hydration products. This is known as the dilution effect [31, 32].

Studies show that high temperature curing of fly ash (FA) blends with replacement levels up to 30% could be beneficial as it can accelerate the pozzolanic reaction [3]. However, in blends with high FA content (> 30% by weight) with low w/b ratio, the acceleration of pozzolanic reaction at higher temperatures (50 °C) can potentially obstruct the later age clinker hydration by consuming pore water [33, 34]. This implies that the effect of temperature on fly ash blends depends on replacement ratio and the water to binder ratio. The incorporation of slag also increases temperature sensitivity [35–37]. As temperature increases, the early age strength increases and this improvement is more at higher replacement levels. Although high temperature curing can affect the ultimate strength, the detrimental impact on strength reduces with increase in slag content [36, 38]. In low clinker blends, the temperature sensitivity of FA is higher than that of slag [39]. Curing of blends incorporating metakaolin at higher temperatures, leads to an increase in the formation of AFm phases due to the increase in the Al_2O_3/SO_3 ratio, increasing temperature sensitivity of the blend [40]. Limestone, another commonly used SCM used as clinker substitution, accelerates the early hydration of clinker due to the filler and dilution effects. The presence of limestone contributes to the formation of carboaluminate phases and prevents the conversion of ettringite to monosulphate [41, 42]. Since, both carboaluminate and ettringite phases are more soluble at higher temperatures, the addition of limestone to cement makes them more sensitive to changes in temperature [2].

Despite extensive research on cement hydration at different temperatures, the hydration behaviour of ternary blended cements is unclear. Particularly, no study on the influence of high-temperature curing on LC^3 was found. This paper focuses on understanding



the difference in the characteristics of C–S–H and the cement microstructure in general when ternary blended cements such as slag-fly ash cement and LC³ are cured isothermally at 27 °C and 50 °C. The formation of various hydrate phases has also been followed and the results have been compared with ordinary Portland cement.

2 Experimental programme

2.1 Materials

The clinker, clay and limestone used in this study were obtained from the state of Gujarat. Ground granulated blast furnace slag was obtained from the state of Goa and fly ash from the state of Uttar Pradesh. The clay, which contained approximately 63% kaolinite content was calcined in a rotary kiln with an air temperature of 900 °C. Details of the calcination process can be found in [43]. Natural gypsum obtained from Oman was used in this study. Indian standard sand [44], obtained from Ennore in Tamil Nadu, were used for making mortar cubes for compressive strength test. The particle size distribution, chemical composition and phase composition of raw materials can be found in supplementary content to this article. Distilled water was used for preparation of the mixes.

First, OPC was produced by intergrinding clinker with gypsum in a 20 kg capacity laboratory ball mill. The other materials used for making blends were ground individually. The other blends used in this study are slag-fly ash composite cement (CC) and limestone calcined clay cement (LC³), were produced by blending the ground raw materials in a turbo-blender. Two LC³ blends were prepared by changing the dosage of gypsum to understand the influence of sulphate content on the hydration behaviour of the alumina rich system. The OPC contained 95% clinker and around 5% gypsum, while the CC and LC³ systems contained 50% clinker. While CC contained 30% slag and 15% fly ash, LC³ contained 30% calcined clay and 15% limestone. Both CC and LC³ (LC³–5%G) contained 5% gypsum, a blend of LC³ with 8% gypsum (LC³–8%G) was also used.

2.2 Preparation of mix and curing conditions

The temperatures of 27 °C and 50 °C were chosen for this study. While 27 °C is the standard curing temperature prescribed in the Indian standards, 50 °C was chosen since it has been reported in the literature that the solubilities of ettringite and carbo-aluminates, which are two important products in LC³, significantly increase above 45 °C [45]. Two types of specimens: paste and mortar cubes were cast. Before casting of the specimens, all the mix materials (cement blends, water and sand) were preconditioned at the required temperature for 24 h. Immediately after casting, mortar cubes were placed in a temperature-controlled curing chamber in closed boxes containing wet jute cloths to avoid drying. The specimens were then demoulded and cured under lime water in a temperature controlled water bath till the time of testing. After 1 day, the specimens were demoulded and placed in a water bath. The water in the temperature-controlled bath was saturated with lime to avoid leaching of calcium hydroxide from the specimens. The specimens were taken at selected ages for testing. Paste mixes were prepared by mixing preconditioned cement blend and distilled water using a high-speed mixer at 2000 rpm for 3 min. The water to binder ratio (w/b ratio) of the mix was kept constant as 0.45 by weight. The fresh mix was then poured in a cylindrical plastic mould of 3 cm diameter and 10 cm length. The moulds were sealed and cured at 27 °C and 50 °C, separately. Slices of 3 mm thickness were cut from the hardened paste samples at the required ages for testing.

3 Test methods

3.1 Isothermal calorimetry

Heat of hydration was measured on fresh paste samples with w/b ratio of 0.45, using isothermal conduction calorimeter (I-Cal 8000, Calmetrix, MA, USA). Before mixing, the cement blend, water and all the containers used for mixing were preconditioned for 24 h at the set temperature. The preconditioned materials were then mixed with distilled water in a plastic cup outside the calorimeter for 3 min using a high-speed paste mixer. 72.5 g of freshly mixed paste (50 g of the dry blend at 0.45 w/b ratio) was then

immediately poured into a plastic cup, which was immediately transferred to the isothermal calorimeter. Logging of readings started from the time of placing of the samples for 3 days. The recorded readings were then exported and represented as heat flow and total heat of hydration per gram of binder.

3.2 Compressive strength

Mortar compressive strength test was measured as described in the standard IS 4031-6 1988. Cube moulds of 7.06 cm size were used to prepare mortar specimens. A cement to sand ratio of 1:3 by weight with a fixed *w/b* ratio of 0.45 was used for making the mix. The curing conditions for the specimens have been discussed in Sect. 2.2. Compressive strengths of the specimens were measured at 3, 7 and 28 days. The average of the peak stresses of three specimens was used to determine the compressive strength of the samples.

3.3 Electron microscopy

For microstructure and mineralogical studies, slices of 3 mm thickness were cut from paste specimens, and the hydration of the samples was stopped using solvent exchange in isopropanol for 5 days, followed by storage of the specimens in vacuum desiccator till the time of testing to avoid carbonation and possibility of further hydration. Although no moisture absorbent was placed in the desiccator, the air was removed using a vacuum pump. Impregnation of the specimen was done with a low viscosity epoxy resin under vacuum. Polishing of the test surface was carried out using fine diamond powders from 9 to 1/4 μm . The polished specimens were then sputter coated with carbon before the imaging. All the analyses were carried out using FEI Quanta 200 SEM (Thermo Fisher Scientific) (15 kV of accelerating voltage, 12.5 mm of working distance) with Bruker XFlash 4030EDS detector. Energy dispersive X-ray spectrometry (EDS) was carried out to study the elemental composition of the specimens and the quantification of the data was carried out using reference oxide minerals.

The relative brightness of the hydration products around the cement grains in the micrographs was quantified in order to understand the influence of temperature on its density. This hydration product is

expected to be mainly C–S–H in the case of OPC and C–A–S–H (calcium aluminosilicate hydrate) in the case of the blended cements in this study. It has been reported that in the case of C–S–H, the grey level is influenced by its microporosity, water content and chemical compositions [24]. The grey-levels of portlandite and the residual belite in all images were normalised to the same level and the grey-levels of the inner product were then compared using an image-analysis software. Portlandite and belite were chosen since their densities and compositions are not expected to significantly change with a change in the curing temperature. Although in the literature, alite is often used for the normalisation, in this study, belite was used since the cement used contained a larger amount of belite and significant unhydrated amounts of belite were present at 28 days. For each blend, 100 images were collected, the grey level of the C–S–H around the cement grain was calculated and respective graphs of frequency% versus grey level were plotted. The relative brightness of C–S–H was calculated according to the formula below [21]:

$$RB_{C-S-H} = \frac{I_{C_2S} - I_{CH}}{I_{C_2S} - I_{C-S-H}}$$

where RB is the ‘Relative Brightness’ and I_{C_2S} and I_{CH} are intensity (grey level) of C_2S and CH. I_{C-S-H} is the intensity (grey level) of C–S–H that was taken as the average of grey scale values in each blended cement.

3.4 Mercury intrusion porosimetry (MIP)

MIP was performed using Thermo Fischer Pascal 440 porosimeter. At the age of testing, i.e. 28 days in this study, the paste slice samples were immersed in isopropanol for 5 days and then stored in a vacuum desiccator till 28 days. About 1.5 to 2 gain of paste samples were cut from the slices after removing the edges. MIP was carried out by measuring the volume of mercury intruded in the specimen as the pressure was incrementally increased to 400 MPa. A contact angle of 120° assumed [46] for the calculation of overall porosity and pore entry diameter. The total percolated pore volume (total/overall porosity) represents the total accessible pore volume at 400 MPa applied pressure and critical pore-entry diameter is the pore size where steepest slope of the cumulative intrusion curve is recorded.



3.5 X-ray diffraction-Rietveld analysis

X-ray diffraction (XRD) was carried out on 3 mm thickness hydrated paste specimen. Prior to the experiment, the cut paste slices were polished using silicon carbide paper to make the surface smooth. Scanning was done immediately after slicing and polishing to avoid carbonation. The experiment was conducted using D8 Advance Eco X-ray diffractometer from Bruker at a voltage of 40 mV and current of 25 mA, with a Cu-K α radiation ($\lambda = 1.54 \text{ \AA}$) and a fixed divergence slit of 0.5° . The specimens were scanned in the range of 5° to 65° at the rate of $0.019^\circ/0.3 \text{ s}$. The quantification of clinker and other phases using Rietveld refinement was carried out using TOPAS software and Bruker Cement Database 2006. Rutile having 98% purity was used as an external standard for quantifying the phases in the hydrated specimens. Scanning of rutile was carried out with each set of data acquisition [47, 48].

4 Results

4.1 Hydration

Heat of hydration of blends cured at 27°C and 50°C are shown in Fig. 1. Although the clinker content in blended cements is approximately half of that in OPC, the peak-heat of LC³ systems is similar to OPC at both temperatures. The induction period of LC³ is shorter as compared to OPC and CC systems at both temperatures. In OPC, acceleration started at around 2 h, and in LC³-5%G, it started around 1 h 30 min. This can be attributed to the nucleation effect of clay fine particles as well as amorphous alumino-silicate content in the clay. The physical influence of the higher surface area

of the calcined clay may also have a role to play in this. Whereas in CC, the acceleration was found to start later than OPC and the peak heat of hydration was lower than OPC, mainly due to lower clinker content and slow pozzolanic activity of both slag and fly ash. A clear aluminate hydration peak is visible in both blended systems, with calcined clay and slag contributing to aluminates in the solution. It is seen in the LC³ blends that the addition of gypsum delays the onset of this peak.

The heat of hydration patterns for 50°C curing emphasises that the heat of hydration increases significantly with the increase in temperature. While at 27°C , the second peak, which usually indicates the hydration of the aluminate phase, is not clearly visible in the case of OPC, it becomes prominent at 50°C . In the LC³ system with 5% gypsum, there appears to be an acceleration in the formation of ettringite and also its conversion to monosulphate, visible as a shoulder after the aluminate peak. However, this shoulder is absent in LC³ with 8% gypsum, indicating that due to the presence of additional sulphates, the conversion of ettringite to monosulphoaluminate is delayed. As shown in Sect. 4.4, this observation was also confirmed by XRD measurements. It can be observed that, when curing was done at 50°C , there is very little additional heat of hydration in the LC³ and CC systems after 24 h of hydration (Fig. 2), indicating a significant reduction in the rate of clinker hydration after 1 day.

4.2 Mortar compressive strength

Figure 3 shows the compressive strength of the mortar cubes cured at 27°C and 50°C up to 28 days. From 7-days onwards, the strength of mortars cured at the higher temperature was found to be lower than the specimens cured at 27°C . While this difference in

Fig. 1 Heat flow of blends cured at 27°C and 50°C

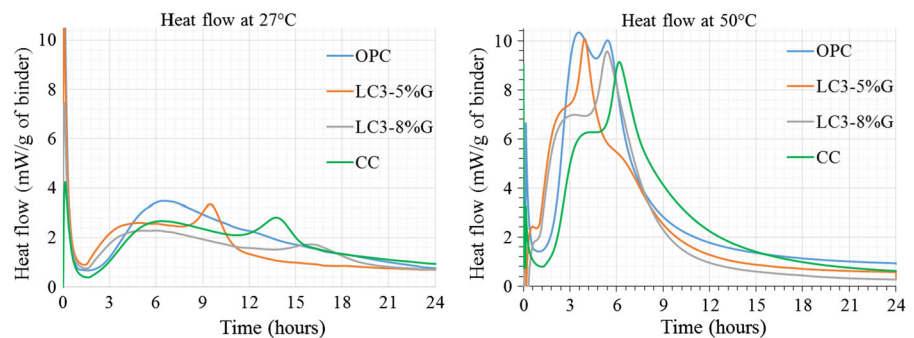


Fig. 2 Heat of hydration of blends cured at 27 °C and 50 °C

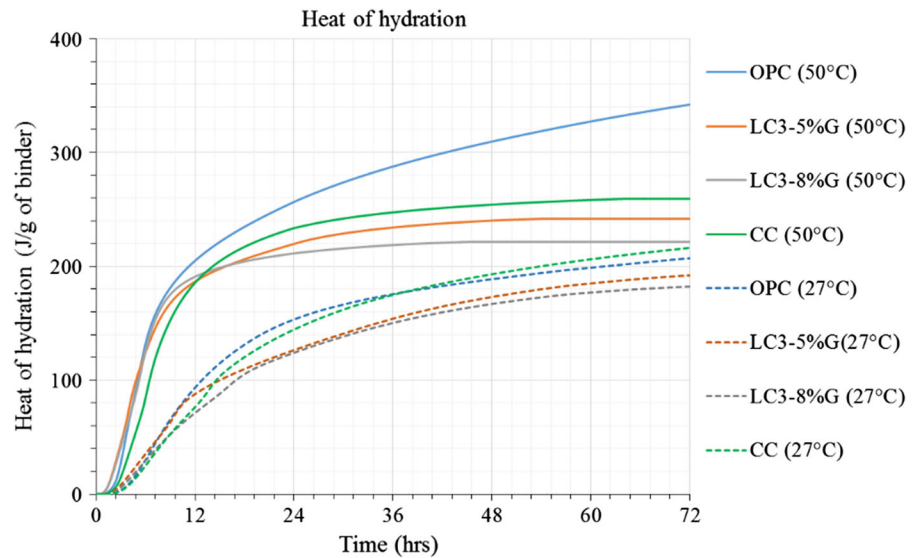
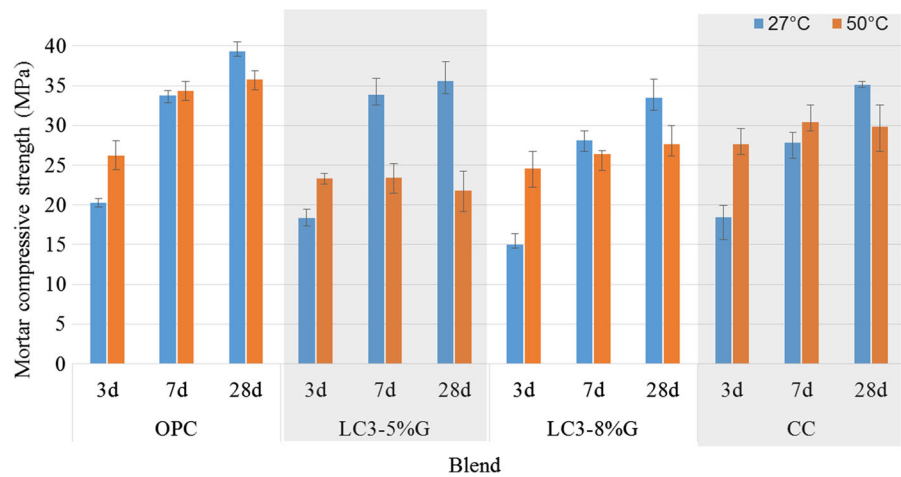


Fig. 3 Compressive strength of mortar cubes cured at 27 °C and 50 °C



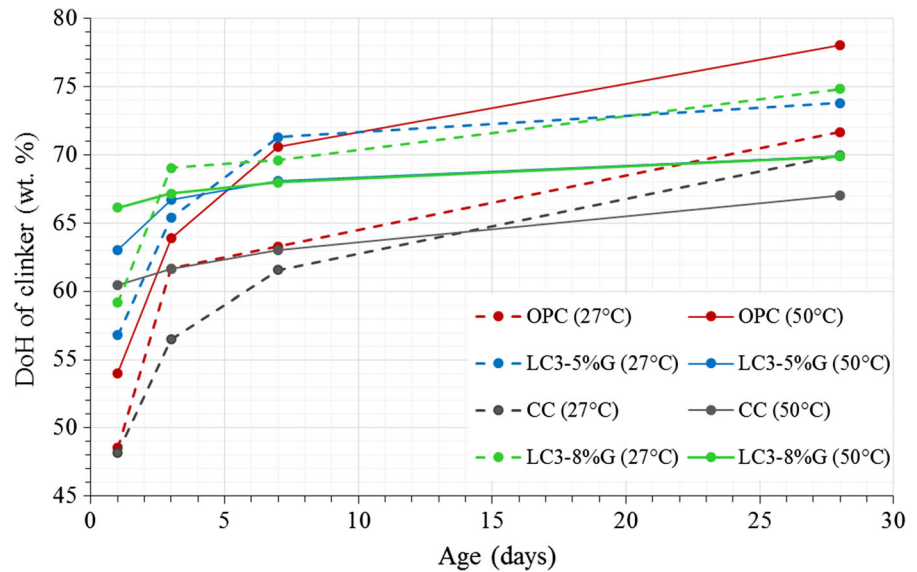
strengths is the least in OPC, it is the highest in LC³ with 5% gypsum. Although the increase in gypsum content slows down the strength development in LC³ at 27 °C, the 28-day strength at 50 °C is slightly higher than the blend with 5% gypsum. When compared to the cements cured at 27 °C, at 50 °C, the strength gain after 3 days is negligible for all the low clinker cements.

4.3 Degree of hydration of clinker phases

The degree of hydration (DoH) of clinker phases calculated using X-ray diffraction is shown in Fig. 4. From the results it can be seen that the hydration of clinker phases in LC³ systems is suppressed at 50 °C

compared to that at 27 °C from 7 day onwards. It was also observed that although the overall degree of clinker hydration is similar in OPC and LC³ systems (73 ± 2%) at 27 °C. The degree of clinker hydration in LC³ systems is reduced to around 70%, even though it increases to 78% in the case of OPC at 50 °C. In the case of CC, although there is a reduction in the degree of hydration at 50 °C, when compared to the same cement at 27 °C, the relative reduction in the case of CC is lower than that observed in the case of LC³-5%G. The increase in strength of all systems is fairly in agreement with the increase in degree of hydration of the respective system.

Fig. 4 DoH of clinker in different blends cured at 27 °C and 50 °C (error: $\pm 3\%$)



4.4 Quantification of hydration products: Rietveld analysis

The X-ray diffractograms in Fig. 5 show that there is a significant change in the phase assemblage of the LC³-5%G pastes when the curing temperature is changed. A quantification of the ettringite (Ettr) and hemicarboaluminate (Hc) was carried out using Rietveld analysis as shown in Fig. 6. Monosulphoaluminate (Ms) could not be quantified due to its poor crystalline structure. In the LC³ systems, at 27 °C, clear peaks of ettringite, monocarboaluminate (Mc) and hemicarboaluminate can be seen even at 28 days

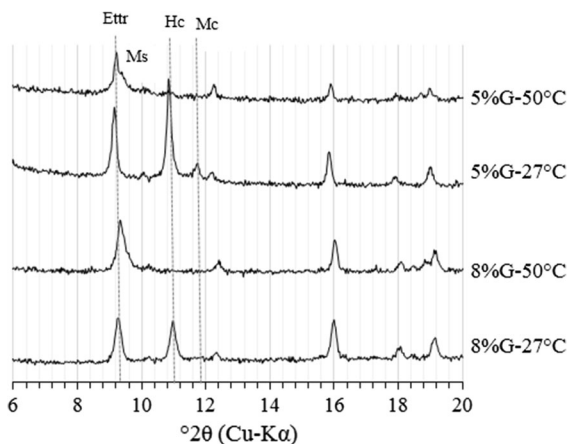


Fig. 5 X-ray diffractograms of LC³ cured at 27 °C and 50 °C at 28 days

for both gypsum contents. However, at 50 °C, a peak of monosulphoaluminate starts to appear, especially in the system with 5% gypsum, and the peaks of the carboaluminate phases are not very clear.

As expected, the increase in gypsum content led to an increase in the ettringite content and a reduction in the hemicarboaluminate content. In the LC³ blend with 5% gypsum cured at 50 °C, the quantity of ettringite reduces with time, as it is probably converted to monosulphoaluminate. A small peak of monosulphoaluminate appears adjacent to the peak of ettringite in this specimen. This conversion is also visible as the third peak in the isothermal calorimetry measurements shown earlier. Compared to LC³ systems cured at 27 °C, a reduction in the quantity of hemicarboaluminate can also be seen and no peak of monocarboaluminate was observed in LC³ systems at 50 °C. The additional sulphates present in the blend with 8% gypsum appear to prevent the conversion of ettringite from occurring, while the quantity of hemicarboaluminate reduces further.

4.5 Quantitative backscattered image analysis

Figure 7 shows the characteristic microstructure of LC³-5%G specimens cured isothermally at 27 °C and 50 °C at 28 days from SEM-BSE images. The images of other specimens can be found in supplementary content to this article. Since there is a relatively large difference in the degrees of hydration of clinker phases

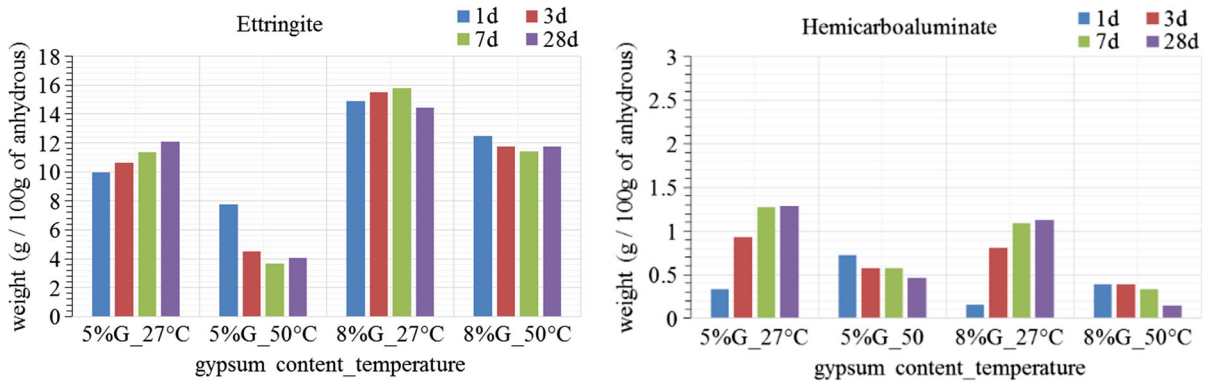


Fig. 6 XRD quantification of ettringite (left) and hemicarboaluminate (right) of LC³ blends (error: ± 1 g)

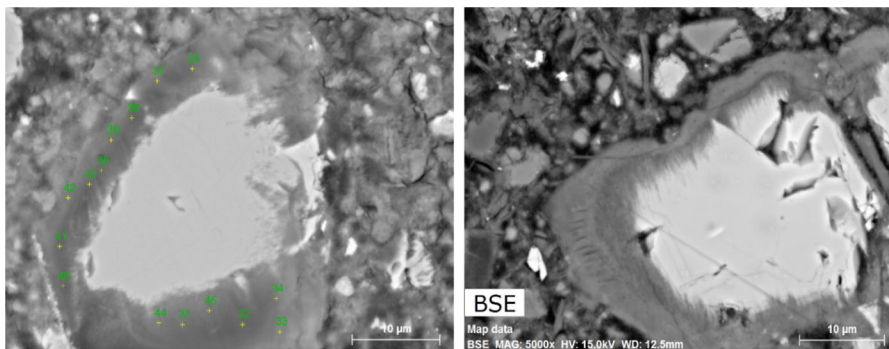


Fig. 7 Backscattered images of LC³-5%G cured at 27 °C (left) and 50 °C (right) at 28 days

at early ages between 27 and 50 °C, a comparison of the microstructures at 28 days is the most relevant for this work. Visually, the microstructure of LC³-5%G cured at 50 °C appears to be more heterogeneous than that cured at 27 °C. It was observed that at the higher temperature, a clear ring of a hydration product, probably C-A-S-H, with a large difference in brightness from the remaining inner product, is seen around the clinker grains in LC³-5%G. A hydration product with a relatively lower brightness can also be seen inside this ring. To have a better understanding on the influence of curing temperature on the brightness and therefore the relative densities of C-A-S-H, the histograms of the grey levels of the product were plotted in Fig. 8. The histogram of CC and LC³-8%G can be found in supplementary materials of this article. It can be seen in this figure that, as has been reported, in the case of OPC and CC the relative brightness of C-A-S-H is higher at 50 °C. A wider distribution of the brightness of C-A-S-H was observed in the LC³ samples. This could be due to the higher intermixing

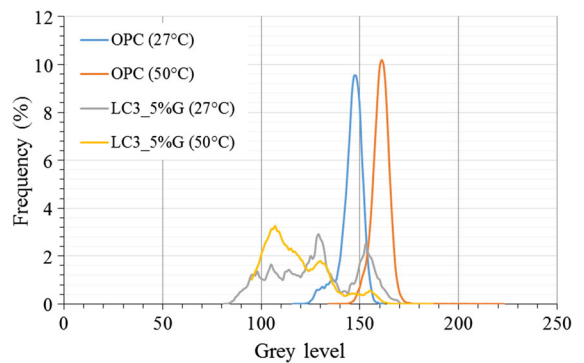
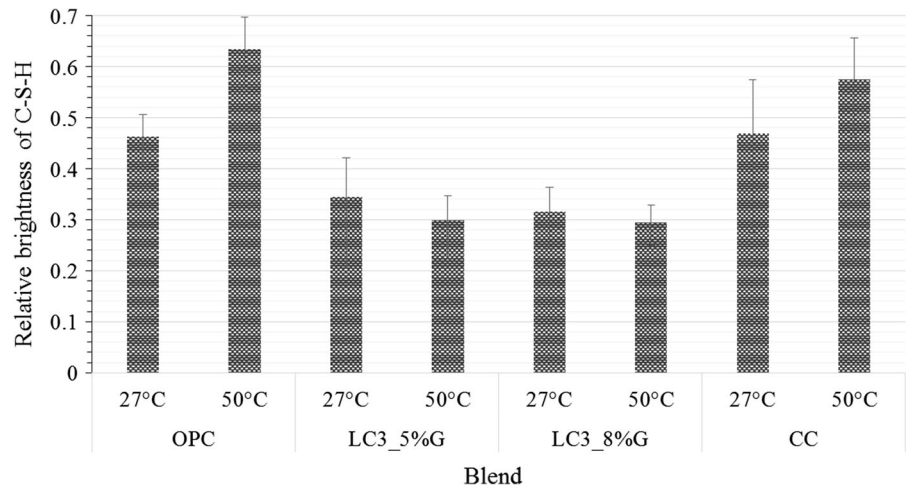


Fig. 8 Histogram of % frequency of grey levels of C-S-H in OPC and LC³-5%G at 28 days

of other products with C-A-S-H in LC³ systems, as has been reported earlier [49]. While a relatively loosely packed C-A-S-H is visible around the clinker grains in LC³, a higher density material appears to form farther from the dissolving surface of the cement particles. As can be seen in Fig. 9, this leads to a reduction in the mean relative brightness of the

Fig. 9 Mean relative brightness of C–S–H in blended cement



product in the case of LC³. Furthermore, while there appears to be a reduction in the variation of the relative brightness at 50 °C, an increase in the average density of the hydration product was not observed. No significant influence of additional sulphate was observed on the mean brightness of the hydration product.

4.6 Elemental analysis (BSE-EDX)

BSE-EDX analysis was carried out on the inner products for all pastes. The spread of the elemental ratios observed for OPC and LC³-5%G are shown in Figs. 10, 11 respectively. The plots for CC and LC³-8%G can be found in the supplementary content to this article. There is a slight reduction in the Ca/Si ratio of all pastes when the temperature is increased. While, there is little influence of temperature on the Al/Si

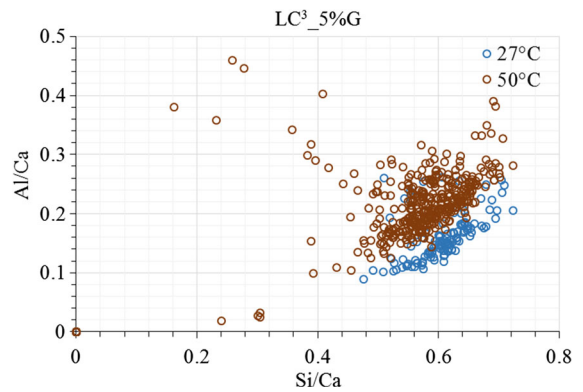


Fig. 11 C–A–S–H composition for LC³-5%G cured at 27 °C and 50 °C at 28 days of hydration obtained by SEM–EDX

ratio of C–A–S–H in the case of OPC and CC, there is a significant increase in the Al/Si ratio with the increase in temperature in the case of LC³. This increase in the alumina content is at the cost of the quantities of ettringite and carboaluminate phases. Despite the increase in the formation of ettringite at 50 °C in the case of 8% gypsum, the Al/Si ratio in C–A–S–H remains unchanged. This indicates that the uptake of alumina in C–A–S–H is preferred to the formation of carboaluminate phases.

4.7 Porosity

Figure 12 shows the influence of temperature on the pore-structure of the pastes hydrated up to 28 days using mercury intrusion porosimetry. In these graphs, the peak value in the y-axis is considered to be the pore volume and the value in the x-axis denoted as the pore-

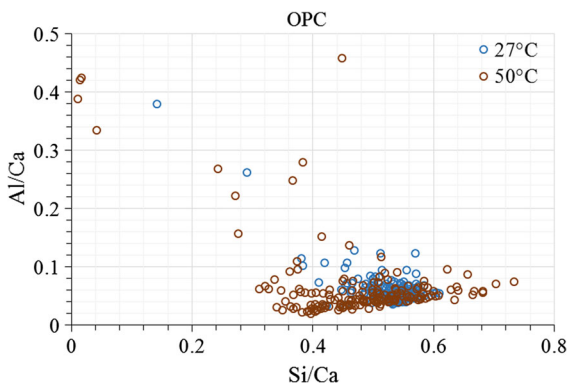


Fig. 10 C–A–S–H composition for OPC cured at 27 °C and 50 °C at 28 days of hydration obtained by SEM–EDX



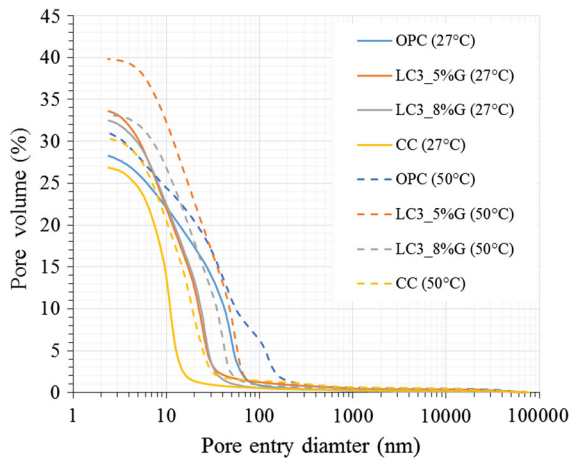


Fig. 12 Porosity graph of different blends cured at 27 and 50 °C at 28 days

entry diameter. In all systems studied, the increase in temperature led to an increase in the overall porosity and the pore-entry diameter. In the case of OPC and CC, while there is a small increase in the total porosity, the increase in the pore entry diameter is large. These changes can be explained by the increase in the density of C–S–H that were observed in the quantitative-BSE analysis. In the case of LC³ with 5% gypsum, there is a large increase in the total porosity. However, when the gypsum content is increased to 8%, the total porosity is comparable with the other blends, perhaps due to the increased formation of ettringite. The small increase in porosity observed in this system can be attributed to the reduction of the carboaluminate phases.

5 Discussion

The influence of an increase of curing temperature from 27 to 50 °C on the hydration and microstructural development of LC³ systems was studied and compared with OPC and CC. It was seen that while even at 27 °C, the characteristics of C–A–S–H in LC³ systems appear to be different from that of OPC and CC, these differences are more exaggerated at 50 °C. While in the case of OPC, it has been reported in the literature that there is a relatively narrow distribution of the composition of C–S–H [8], in the case of LC³, an intermixing of the hydration products is apparent in the wider variation of the composition of C–A–S–H. The inner product in the case of LC³ also appears to be

less dense than in the case of OPC and CC. At 50 °C, the reduced formation of aluminate phases in LC³ was found to lead to a significant increase in the aluminate content in the C–A–S–H. This observation is supported by the findings in the literature that ettringite and sulfoaluminate phases are more soluble at higher temperatures, leading to an increase in the alumina in the C–A–S–H [27].

The results in this article shed interesting light on the hydration and microstructural development of LC³. The wider distribution of the composition of C–A–S–H, the finer pores despite similar values of porosity and lower brightness of C–A–S–H compared to OPC, suggest that the hydration product in LC³ is more uniformly distributed throughout the microstructure. The presence of large quantities of ettringite and other products with high surface area such as the carboaluminates would promote the nucleation and growth of C–A–S–H on their surface. Since these one-dimensional and two-dimensional products would tend to grow more rapidly away from the surface of the cement grains, the hydration products will be distributed farther away. The growth of C–S–H away from the cement particles, and on the framework of AFt needles has been suggested in the literature [50]. This is also consistent with the finding that the hydration products are more intermixed in the case of LC³ [49]. This would not only explain the lower packing density of the product, but also the finer pores in the microstructure.

The observation that the ultimate degrees of hydration of alite and belite in LC³ (reference: supplementary content to this article) are lower than those in OPC indicate that a barrier to hydration exists at later ages. It has been reported in the literature that there is a higher polymerisation of C–A–S–H at higher Al to Si ratios and at lower Ca to Si ratios as is the case in LC³ [4, 51, 52]. This polymerisation would hinder the flow of water and ions through the hydration product, slowing down the rate of hydration. While at lower temperatures a more uniform distribution of the product takes place, it has been reported that C–A–S–H tends to deposit closer to the cement grains at higher temperatures [21]. As observed in the experimental results, this leads to a further reduction in the degrees of hydration of alite and belite, and also in a coarsening of the pore-structure. The reduction in ettringite and sulfoaluminate phases, which are lower density phases that lead to a significant

reduction in the porosity, at the higher temperature, also contributes to an increase in the total porosity. All the above contribute to a reduction in the compressive strength of LC³ mortars when curing is carried out at 50 °C. Most importantly, the results clearly show that the LC³ is more sensitive to curing at higher temperatures than OPC and CC.

It may be noted here that although the above discussion is speculative in nature, the relatively simple explanation can satisfactorily explain all the important observations in this study. Further work may be required to understand the distribution of hydration products in hydrating LC³ pastes.

6 Conclusions

The main conclusions that can be drawn from this study are listed below.

1. While the reduction in strength of OPC and CC with the increase in temperature can be attributed mostly to the increase in the density of C–A–S–H, in the case of LC³, this reduction appears to be more due to the suppression of hydration of clinker phases beyond 24 h and the reduction of ettringite and carboaluminate phases.
2. The C–A–S–H formed in LC³ appears to be more mixed with other products and more homogeneously distributed throughout the microstructure, leading to finer pores. However, the distribution of the product becomes more heterogeneous at 50 °C leading to a coarsening of the pores, despite there not being a significant change in the density of the product.
3. The higher alumina uptake in C–A–S–H in the case of LC³, appears to lead to a higher level of polymerisation of the product. The lower degrees of hydration of the clinker phases at 28 day indicate that, perhaps due to this polymerisation, this product hinders the flow of water and ions through it. This effect appears to be more pronounced at 50 °C, where more of polymerised hydration product deposits near the cement grains.
4. Although there is an increase in the ettringite content upon the addition of gypsum to LC³, a reduction in the carbo-aluminate phases takes place, while the alumina substitution in C–A–S–H appears to remain unchanged.

Although some of the conclusions above are speculative in nature, they provide an explanation to most of the important observations in this study. However, further work is required for verification.

Acknowledgements The authors would like to acknowledge the financial support from the Swiss Agency for Development and Cooperation (SDC) and Prof. Karen Scrivener for allowing access of the laboratory at École Polytechnique Fédérale de Lausanne (EPFL), Switzerland. Funding was provided by Direktion für Entwicklung und Zusammenarbeit.

Compliance with ethical standards

Conflict of interest The authors declare that they have no conflict of interest.

References

1. Mahasanen N, Smith S, Humphreys K (2003) The cement industry and global climate change: current and potential future cement industry CO₂ emissions. In: Gale J, Kaya Y (eds) 6th International conference on greenhouse gas control technologies. Pergamon, Oxford, pp 995–1000. <https://doi.org/10.1016/B978-008044276-1/50157-4>
2. Lothenbach B, Winnefeld F, Alder C, Wieland E, Lunk P (2007) Effect of temperature on the pore solution, microstructure and hydration products of portland cement pastes. *Cem Concr Res* 37:483–491. <https://doi.org/10.1016/j.cemconres.2006.11.016>
3. De Weerd K, Ben Haha M, Le Saout G, Kjellsen KO, Justnes H, Lothenbach B (2012) The effect of temperature on the hydration of composite cements containing limestone powder and fly ash. *Mater Struct Constr* 45:1101–1114. <https://doi.org/10.1617/s11527-011-9819-5>
4. Deschner F, Lothenbach B, Winnefeld F, Neubauer J (2013) Effect of temperature on the hydration of Portland cement blended with siliceous fly ash. *Cem Concr Res* 52:169–181. <https://doi.org/10.1016/j.cemconres.2013.07.006>
5. Escalante-García J, Sharp J (1998) Effect of temperature on the hydration of the main clinker phases in portland cements: part I, neat cements. *Cem Concr Res* 28:1245–1257. [https://doi.org/10.1016/S0008-8846\(98\)00115-X](https://doi.org/10.1016/S0008-8846(98)00115-X)
6. Kjellsen KO, Detwiler RJ, Gjorv OE (1991) Development of microstructures in plain cement pastes hydrated at different temperatures. *Cem Concr Res* 21:179–189. [https://doi.org/10.1016/0008-8846\(91\)90044-I](https://doi.org/10.1016/0008-8846(91)90044-I)
7. Zhang X (2006) Quantitative microstructural characterisation of concrete cured under realistic temperature conditions. <https://doi.org/10.5075/epfl-thesis-3725>
8. Famy C, Scrivener KL, Atkinson A, Brough AR (2002) Effects of an early or a late heat treatment on the microstructure and composition of inner C–S–H products of Portland cement mortars. *Cem Concr Res* 32:269–278. [https://doi.org/10.1016/S0008-8846\(01\)00670-6](https://doi.org/10.1016/S0008-8846(01)00670-6)



9. Bentur A, Berger RL, Kung JH, Milestone NB, Young JF (1979) Structural properties of calcium silicate pastes: II. Effect of curing temperature. *J Am Ceram Soc* 62:362–366
10. Pekins RB, Palmer C (1999) Solubility of ettringite ($\text{Ca}_6[\text{Al}(\text{OH})_6]_2(\text{SO}_4)_3 \cdot 26\text{H}_2\text{O}$) at 5–75°C. *Geochim Cosmochim Acta* 63:1969–1980. <https://doi.org/10.1111/j.1440-1746.2009.06068.x>
11. Lothenbach B, Matschei T, Möschner G, Glasser FP (2008) Thermodynamic modelling of the effect of temperature on the hydration and porosity of Portland cement. *Cem Concr Res* 38:1–18. <https://doi.org/10.1016/j.cemconres.2007.08.017>
12. Hirljac J, Wu ZQ, Young JF (1983) Silicate polymerization during the hydration of alite. *Cem Concr Res* 13:877–886
13. Bach TTH, Coumes CCD, Pochard I, Mercier C, Revel B, Nonat A (2012) Influence of temperature on the hydration products of low pH cements. *Cem Concr Res* 42:805–817. <https://doi.org/10.1016/j.cemconres.2012.03.009>
14. Fraaay ALA, Bijen J, de Haan YM (1989) The reaction of fly ash in concrete. A critical examination. *Cem Concr Res* 19:235–246
15. Escalante-Garcia J, Sharp J (1999) Variation in the composition of C–S–H gel in Portland cement pastes cured at various temperatures. *J Am Ceram Soc* 82:3237–3241. <https://doi.org/10.1111/j.1151-2916.1999.tb02230.x>
16. Vance K, Aguayo M, Oey T, Sant G, Neithalath N (2013) Hydration and strength development in ternary Portland cement blends containing limestone and fly ash or meta-kaolin. *Cem Concr Compos.* <https://doi.org/10.1016/j.cemconcomp.2013.03.028>
17. Damidot D, Glasser FP (1992) Thermodynamic investigation of the $\text{CaO}-\text{Al}_2\text{O}_3-\text{CaSO}_4-\text{H}_2\text{O}$ system at 50°C and 85°C. *Cem Concr Res* 22:1179–1191. [https://doi.org/10.1016/0008-8846\(92\)90047-Y](https://doi.org/10.1016/0008-8846(92)90047-Y)
18. Kjellsen KO, Detwiler RJ, Gjörv OE (1990) Backscattered electron imaging of cement pastes hydrated at different temperatures. *Cem Concr Res* 20:308–311. [https://doi.org/10.1016/0008-8846\(90\)90085-C](https://doi.org/10.1016/0008-8846(90)90085-C)
19. Scrivener KL (1992) The effect of heat treatment on inner product C–S–H. *Cem Concr Res* 22:1224–1226. [https://doi.org/10.1016/0008-8846\(92\)90051-V](https://doi.org/10.1016/0008-8846(92)90051-V)
20. Famy C, Scrivener KL, Crumie AK (2002) What causes differences of C–S–H gel grey levels in backscattered electron images? *Cem Concr Res.* [https://doi.org/10.1016/S0008-8846\(02\)00808-6](https://doi.org/10.1016/S0008-8846(02)00808-6)
21. Gallucci E, Zhang X, Scrivener KL (2013) Effect of temperature on the microstructure of calcium silicate hydrate (C–S–H). *Cem Concr Res* 53:185–195. <https://doi.org/10.1016/j.cemconres.2013.06.008>
22. Bahafid S, Ghabezloo S, Duc M, Faure P, Sulem J (2017) Effect of the hydration temperature on the microstructure of Class G cement: C–S–H composition and density. *Cem Concr Res* 95:270–281. <https://doi.org/10.1016/j.cemconres.2017.02.008>
23. Odler I, Abdul-Maula S, Zhongya L (1986) Effect of hydration temperature on cement paste structure. In: *MRS proceedings*, pp 139–144. <https://doi.org/10.1557/proc-85-139>
24. Lewis M, Scrivener K, Kelham S (1994) Heat curing and delayed ettringite formation. *MRS Proc* 370:67. <https://doi.org/10.1557/PROC-370-67>
25. Yang R, Lawrence CD, Lynsdale CJ, Sharp JH (1999) Delayed ettringite formation in heat-cured Portland cement mortars. *Cem Concr Res* 29:17–25. [https://doi.org/10.1016/S0008-8846\(98\)00168-9](https://doi.org/10.1016/S0008-8846(98)00168-9)
26. Ramlochan T, Thomas MDA, Hooton RD (2004) The effect of pozzolans and slag on the expansion of mortars cured at elevated temperature: part II: microstructural and micro-chemical investigations. *Cem Concr Res* 34:1341–1356. <https://doi.org/10.1016/j.cemconres.2003.12.026>
27. Barbarulo R, Peycelon H, Leclercq S (2007) Chemical equilibria between C–S–H and ettringite, at 20 and 85°C. *Cem Concr Res* 37:1176–1181. <https://doi.org/10.1016/j.cemconres.2007.04.013>
28. Francis Young J (1988) Investigations of calcium silicate hydrate structure using silicon-29 nuclear magnetic resonance spectroscopy. *J Am Ceram Soc* 71:C-118–C-120. <https://doi.org/10.1111/j.1151-2916.1988.tb05028.x>
29. Cong X, Kirkpatrick RJ (1995) Effects of the temperature and relative humidity on the structure of C–S–H gel. *Cem Concr Res* 25:1237–1245. [https://doi.org/10.1016/0008-8846\(95\)00116-T](https://doi.org/10.1016/0008-8846(95)00116-T)
30. Jennings HM, Thomas JJ, Gevrenov JS, Constantinides G, Ulm FJ (2007) A multi-technique investigation of the nanoporosity of cement paste. *Cem Concr Res* 37:329–336. <https://doi.org/10.1016/j.cemconres.2006.03.021>
31. Guteridge WA, Dalziel JA (1990) Filler cement: the effect of the secondary component on the hydration of Portland cement—part 2: fine hydraulic binders. *Cem Concr Res* 20:853–861
32. Cyr M, Lawrence P, Ringot E (2005) Mineral admixtures in mortars quantification of the physical effects of inert materials on short-term hydration. *Cem Concr Res* 35:719–730. <https://doi.org/10.1016/j.cemconres.2004.05.030>
33. Maltais Y, Marchand J (1997) Influence of curing temperature on cement hydration and mechanical strength development of fly ash mortars. *Cem Concr Res* 27:1009–1020. [https://doi.org/10.1016/S0008-8846\(97\)00098-7](https://doi.org/10.1016/S0008-8846(97)00098-7)
34. Narmluk M, Nawa T (2011) Effect of fly ash on the kinetics of Portland cement hydration at different curing temperatures. *Cem Concr Res* 41:579–589. <https://doi.org/10.1016/j.cemconres.2011.02.005>
35. Escalante JI, Gómez LY, Johal KK, Mendoza G, Mancha H, Méndez J (2001) Reactivity of blast-furnace slag in Portland cement blends hydrated under different conditions. *Cem Concr Res* 31:1403–1409. [https://doi.org/10.1016/S0008-8846\(01\)00587-7](https://doi.org/10.1016/S0008-8846(01)00587-7)
36. Barnett SJ, Soutsos MN, Millard SG, Bungey JH (2006) Strength development of mortars containing ground granulated blast-furnace slag: effect of curing temperature and determination of apparent activation energies. *Cem Concr Res* 36:434–440. <https://doi.org/10.1016/j.cemconres.2005.11.002>
37. Castellano CC, Bonavetti VL, Donza HA, Irassar EF (2016) The effect of w/b and temperature on the hydration and strength of blastfurnace slag cements. *Constr Build Mater* 111:679–688. <https://doi.org/10.1016/j.conbuildmat.2015.11.001>
38. Liao WC, Lee BJ, Kang CW (2008) A humidity-adjusted maturity function for the early age strength prediction of



- concrete. *Cem Concr Compos* 30:515–523. <https://doi.org/10.1016/j.cemconcomp.2008.02.006>
39. Xu G, Tian Q, Miao J, Liu J (2017) Early-age hydration and mechanical properties of high volume slag and fly ash concrete at different curing temperatures. *Constr Build Mater* 149:367–377. <https://doi.org/10.1016/j.conbuildmat.2017.05.080>
40. Williams A, Markandeya A, Stetsko Y, Riding K, Zayed A (2017) Cracking potential and temperature sensitivity of metakaolin concrete. *Constr Build Mater* 120:172–180. <https://doi.org/10.1016/j.conbuildmat.2016.05.087>
41. Lothenbach B, Le Saout G, Gallucci E, Scrivener KL (2008) Influence of limestone and anhydrite on the hydration of Portland cements. *Cem Concr Compos* 38:848–868. <https://doi.org/10.1016/j.cemconcomp.2013.11.007>
42. Zajac M, Rossberg A, Le G, Lothenbach B (2014) Influence of limestone and anhydrite on the hydration of Portland cements. *Cem Concr Compos* 46:99–108. <https://doi.org/10.1016/j.cemconcomp.2013.11.007>
43. Emmanuel AC, Haldar P, Maity S, Bishnoi S (2016) Second pilot production of limestone calcined clay cement in India: the experience. *Indian Concr J* 90:57–64
44. IS: 650 (1991) Specification for standard sand for testing of cement
45. Thomas JJ, Rothstein D, Jennings HM, Christensen BJ (2003) Effect of hydration temperature on the solubility behavior of Ca-, S-, Al-, and Si-bearing solid phases in Portland cement pastes. *Cem Concr Res* 33:2037–2047. [https://doi.org/10.1016/S0008-8846\(03\)00224-2](https://doi.org/10.1016/S0008-8846(03)00224-2)
46. Muller ACA, Scrivener KL (2017) A reassessment of mercury intrusion porosimetry by comparison with ^1H NMR relaxometry. *Cem Concr Res* 100:350–360. <https://doi.org/10.1016/j.cemconres.2017.05.024>
47. O'Connor BH, Raven MD (1988) Application of the Rietveld refinement procedure in assaying powdered mixtures. *Powder Diffr* 3:2–6. <https://doi.org/10.1017/S0885715600013026>
48. Scrivener K, Snellings R, Lothenbach B (2016) A practical guide to microstructural analysis of cementitious materials. CRC Press, Boca Raton. <https://doi.org/10.7693/wl20150205>
49. Wilson W, Sorelli L, Krishnan S, Bishnoi S, Tagnit-Hamou A (2017) Micro-chemo-mechanical characterization of a limestone-calcined-clay cement paste by statistical nanoindentation and quantitative SEM-EDS. In: Proceedings of the 2nd international conference on calcined clays for sustainable concrete, pp 494–499. https://doi.org/10.1007/978-94-024-1207-9_79
50. Scrivener KL (1984) The development of microstructure during the hydration of Portland cement. University of London, London
51. Hôpital EL, Lothenbach B, Le Saout G, Kulik D, Scrivener K (2015) Incorporation of aluminium in calcium–silicate–hydrates. *Cem Concr Res* 75:91–103. <https://doi.org/10.1016/j.cemconres.2015.04.007>
52. Sun GK, Young JF, Kirkpatrick RJ (2006) The role of Al in C–S–H: NMR, XRD, and compositional results for precipitated samples. *Cem Concr Res* 36:18–29. <https://doi.org/10.1016/j.cemconres.2005.03.002>

Publisher's Note Springer Nature remains neutral with regard to jurisdictional claims in published maps and institutional affiliations.

